Brushless Doubly Fed Machine Magnetic Field Distribution Characteristics and their Impact on the Analysis and Design

Mmamolatelo E. Mathekga, Sul Ademi and Richard A. McMahon

***Abstract*—This paper contributes to the characterisation of the brushless doubly fed induction machine (BDFIM), which is attractive as a variable speed generator in applications (offshore wind turbine) with minimum maintenance requirements. The BDFIM has two three-phase stator windings of different pole numbers housed within the same stator slots and a short-circuited rotor winding capable of coupling fields of different pole numbers. The stator windings and rotor winding create a magnetic field distribution with a range of characteristics different to those of conventional induction machines. This paper presents an analysis to identify the field characteristics and discusses their impact on the analysis and design of the BDFIM. The characteristics are determined from an analysis of the sum of two rotating sinusoidal field waveforms and confirmed by comparison with time-stepping finite element results and measured magnetic flux density data.**

***Index Terms*—Brushless doubly fed machine (BDFM), flux density, field distribution, rotor design, core loss, standing wave.**

I. Introduction

BRUSHLESS doubly fed machines (BDFMs) are attractive for use in wind turbines since they offer improved reliability and reduced capital and maintenance costs compared to the well-established doubly fed induction machine (DFIM) [1]. Employing BDFMs retains the low-cost advantage of the DFIM system as they only require a fractionally rated converter and they do not use permanent magnet materials [2], [3]. BDFMs have no brushed contact to the rotor, eliminating a maintenance requirement, making them particularly attractive for offshore wind turbines [4], [5]. In addition, they are intrinsically medium-speed machines, enabling the use of a simplified one or two stage gearbox. A schematic of a typical drivetrain is shown in Fig. 1.

There are two principle forms of BDFMs, namely the brushless doubly fed reluctance machine (BDFRM) [6], [7] and the brushless doubly fed induction machine (BDFIM) [4], which is the focal point of this paper. The brushless DFIM has its origins in the self-cascaded machine and has two non-coupling stator windings, referred to as the power winding (PW) and the control winding (CW) with different pole numbers, p_1 and p_2, creating two fields in the machine's magnetic circuit [8], [9]. A specially designed rotor couples to both stator windings.

The air-gap magnetic field distribution in the BDFIM has characteristics different to those of an electrical machine with a field distribution of a single pole number, the most obvious being that the form of the field distribution changes as a function of time as it rotates [10], as depicted in Fig. 2. From a stator perspective, it does not have a clearly defined n-pole pattern and that the movement of the field distribution is not a matter of simple rotation [11]. However, in early research work on the self-cascaded machine, the forerunner of the BDFIM, it was found that the field distribution had the interesting characteristic of being stationary in the rotor reference frame and that the amplitudes of the peaks in the field varied sinusoidally with angular position [12], [13].

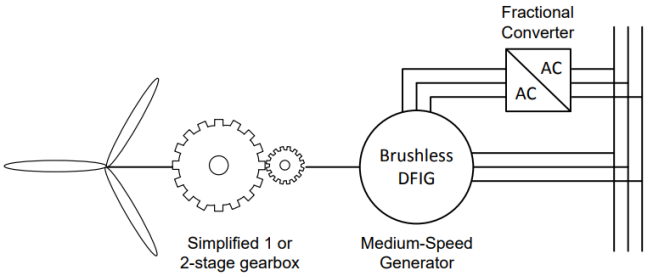

Fig. 1. Brushless DFIM drivetrain set-up for wind power applications.

As a consequence of the field distribution, conventional approaches cannot be used to predict core losses and determine saturation effects in the BDFIM. In particular it has been hard to establish a way of optimizing the magnetic design of these machines [10], [14]. Therefore, this paper examines the field distribution in a BDFIM to understand the impact of the nature of the field distribution on machine design and performance.

II. BDFIM Magnetic Flux Density Distribution

The radially directed air-gap flux density distribution is found from the sum of the two principal fields with p_1 and p_2 poles within the machine, assuming that space harmonics components are small. In the stator reference frame the sum of the two components, with p_1 and p_2 poles, is given by:

$$B(\theta,t) = B_1\cos(2\pi f_1 t - p_1\theta) + B_2\cos(2\pi f_2 t - p_2\theta + \alpha) \quad (1)$$

where B_1 and B_2 are the peak flux density of the $2p_1$-pole and $2p_2$-pole components of the air-gap flux density, respectively, f_1 and f_2 are the excitation frequencies, t is time, θ is the angular position with a range of $(0:2\pi)$ radians. The phase offset α is the combination of the relative physical position of the two stator windings and the operating load angle.

In summary, the form of the field distribution depends on the relative amplitude of the two field components, excitation frequencies and their relative angular offset. The field distribution is a non-sinusoidal function of θ for all t values, and a

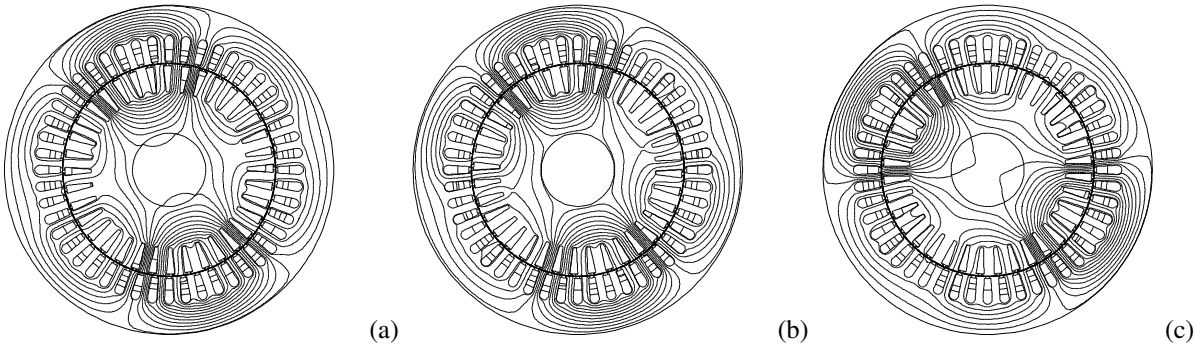

Fig. 2. The magnetic flux distribution of a BDFIM with a 4-pole and a 8-pole stator windings (Frame size D180), operating at 500 rpm in cascade mode with the 4-pole stator winding excited; captured 1 ms apart, in order.

non-sinusoidal function of t for all θ values except in certain special cases considered in section III-A, e.g., $f_1 = 0$ Hz or $f_2 = 0$ Hz. An example is shown in Fig. 3, illustrating changes in flux density as function of θ for different values of t.

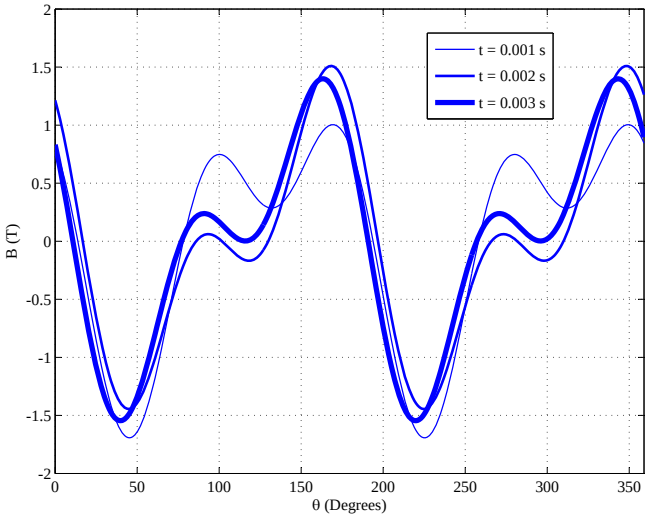

Fig. 3. Graphical representation of equation (1) as a function of θ for consecutive values of t, 1 ms apart with: $f_1 = 50$ Hz, $f_2 = 40$ Hz, $B_1 = 1.0$ T, and $B_2 = 0.7$ T.

III. Field Analysis

Equation (1) is a periodic function with a period, T, that is given by

$$T = \frac{n}{f_1} = \frac{m}{f_2} \tag{2}$$

where: n and m are integers that satisfy the following equation

$$\frac{n}{m} = \frac{f_1}{f_2} \tag{3}$$

In certain circumstances the field distribution assumes particular characteristics as considered below.

A. $f_1 = 0$ Hz or $f_2 = 0$ Hz

In this case equation (1) reduces to the sum of a traveling waveform and a sinusoidal function of θ. The peak values of $B(\theta, t)$ occur at varying angular positions at different times because of the sinusoidal function of θ, which contributes a θ dependent offset to the peak value of the travelling waveform. However, the magnitudes of the peak values are independent of the angular position at which they occur.

B. Frequencies in the Ratio of the Poles

When the values of f_1 and f_2 are related as follows

$$\frac{f_1}{p_1} = \frac{f_2}{p_2} \tag{4}$$

The form of the field distribution does not change as a function of t and rotates around the machine as shown in Fig. 4(a) because the angular velocities of the $2p_1$ and $2p_2$ pole flux density distributions are equal. However, the field distribution as a function of θ, as well as the positive and negative peak values, depend on the relative offset α between the $2p_1$-pole and $2p_2$-pole flux density distributions, which in turn depends on operating conditions. Also, the positive and the absolute negative peak values are different and less than $|B_1 + B_2|$ for most values of α as shown in Fig. 4(b).

C. Integer Ratio Frequencies

Under these conditions equation (1) reduces to the sum of a traveling wave and a standing wave when the values of f_1 and f_2 are related by $f_1 = \pm f_2/i$ and $f_2 = \pm f_1/i$, where i is an integer. For example when $f_1 = f_2$, equation (1) reduces to

$$\begin{aligned} B(\theta, t) = {} & 2B_1 \cos(2\pi f_1 t - 0.5(p_1 + p_2)\theta) \times \cos(0.5(p_2 - p_1)\theta) \\ & + \quad (B_2 - B_1)\cos(2\pi f_1 t - p_2\theta) \end{aligned} \tag{5}$$

The peak values of equation (5) are not equal at each angular position because of the standing wave term:

$$2B_1 \cos\left(0.5(p_2 - p_1)\theta\right) \times \cos\left(2\pi f_1 t - 0.5(p_1 + p_2)\theta\right)$$

The peak values instead vary sinusoidally with angular position at any particular instant in time as shown in Fig. 5 and Fig. 6; where $B^{-,\text{peak}}$ and $B^{+,\text{peak}}$ are the negative and positive peak values of equation (5) as a function of θ. The amplitudes at different θ values are not equal and vary periodically as illustrated in Figs. 6(a) and 6(b) for two frequency ratios. The general forms of $B^{-,\text{peak}}(\theta)$ and $B^{+,\text{peak}}(\theta)$ are deduced from Fig. 6 and they are given by:

$$\begin{aligned} B^{-,\text{peak}}(\theta) &= -a_0 - a_1|\cos\left(k\theta + \beta\right)| \\ B^{+,\text{peak}}(\theta) &= \quad a_0 + a_1|\cos k\theta| \end{aligned} \tag{6}$$

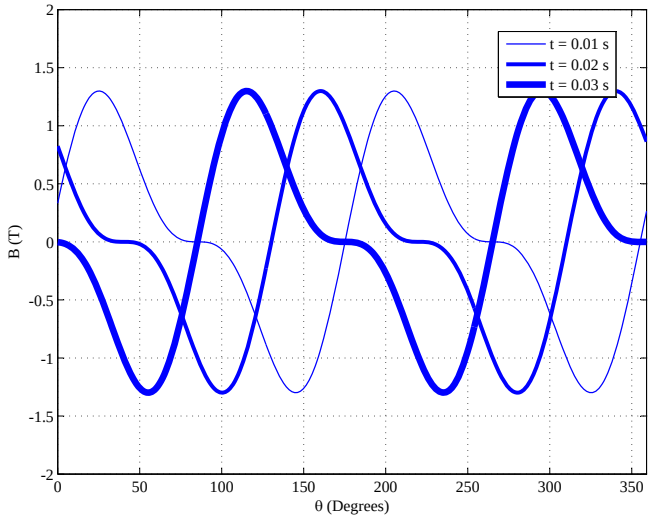

(a)

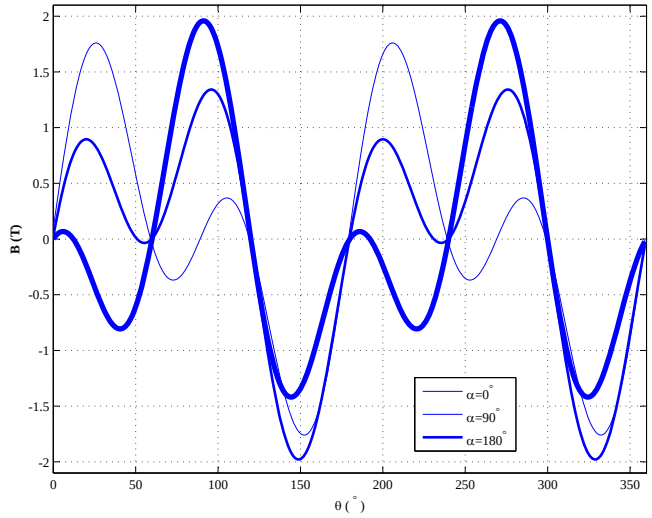

(b)

Fig. 4. Graphical representation of equation (1) as a function of θ with f_1 and f_2 values that are related by equation (4): (a) for consecutive values of t 10 ms apart, and (b) for different relative alignments with α equal to 0, $\pi/2$, and π radians.

where the values of a_0, a_1, k, and β vary with i as detailed in section III(C) and as follows:

- k, the wavenumber, increases with increasing i. This means that the number of angular positions where the values of both $B^{-,\text{peak}}(\theta)$ and $B^{+,\text{peak}}(\theta)$ are equal to $-(B_1 + B_2)$ and $(B_1 + B_2)$ respectively, is proportional to the value of i.
- The value of a_0 increases and that of a_1 decreases as i increases. This is despite their dependence on the amplitudes of the $2p_1$ and $2p_2$ flux density distributions and it means that the variation of the positive and negative peaks values of $B(\theta, t)$ with angular position becomes less significant as i becomes large.
- β is equal to 90° and 0° for even and odd values of i, respectively. This means that the angular positions where the values of $|B^{-,\text{peak}}(\theta)|$ and $|B^{+,\text{peak}}(\theta)|$ are largest, are not the same for even values of i as illustrated in Fig. 6 (a) and (b) as well as Fig. 6 (c) and (d).

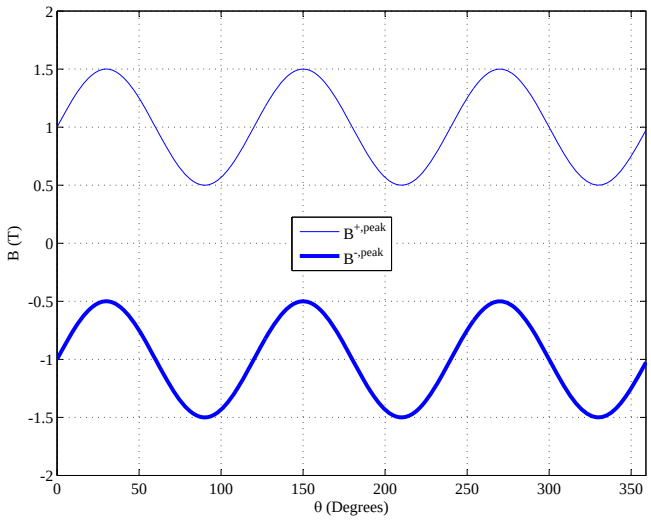

(a)

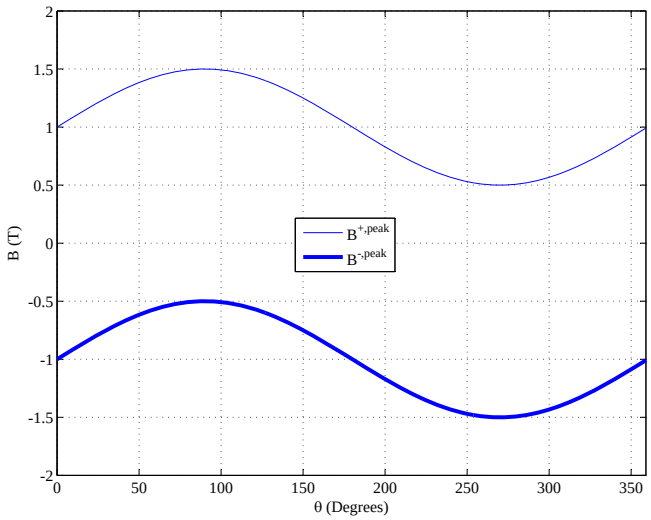

(b)

Fig. 5. Graphical representation of the negative peak values ($B^{-,\text{peak}}(\theta)$) and positive peak values ($B^{+,\text{peak}}(\theta)$) of equation (1) as a function of θ for: (a) $f_2 = 0$ Hz, $B_1 = 1.0$ T, and $B_2 = 0.5$ T as well as (b) $f_1 = 0$ Hz, $B_1 = 0.5$ T, and $B_2 = 1.0$ T.

IV. Characteristics with Reference to the BDFIM

It is clear from section III that the field distribution depends on the relationship between the frequencies of the $2p_1$-pole and $2p_2$-pole stator excitations, i.e. f_1 and f_2. In wind applications the machine would be typically operated with one winding at grid frequency (50 or 60 Hz) with the other winding having a frequency range of around +/- 1/3 of grid frequency. However, in some applications both stator windings may be fed with variable frequencies.

A. Stator Reference Frame Field Distribution Characteristics and Implications

The values of f_1 and f_2 for the stator field distribution components are related by the BDFIM speed equation:

$$N = 60\frac{f_1 \pm f_2}{p} \tag{7}$$

where N is the shaft speed in rev./min. The only practical form of machine has p equal to $p_1 + p_2$ and the two fields rotate in

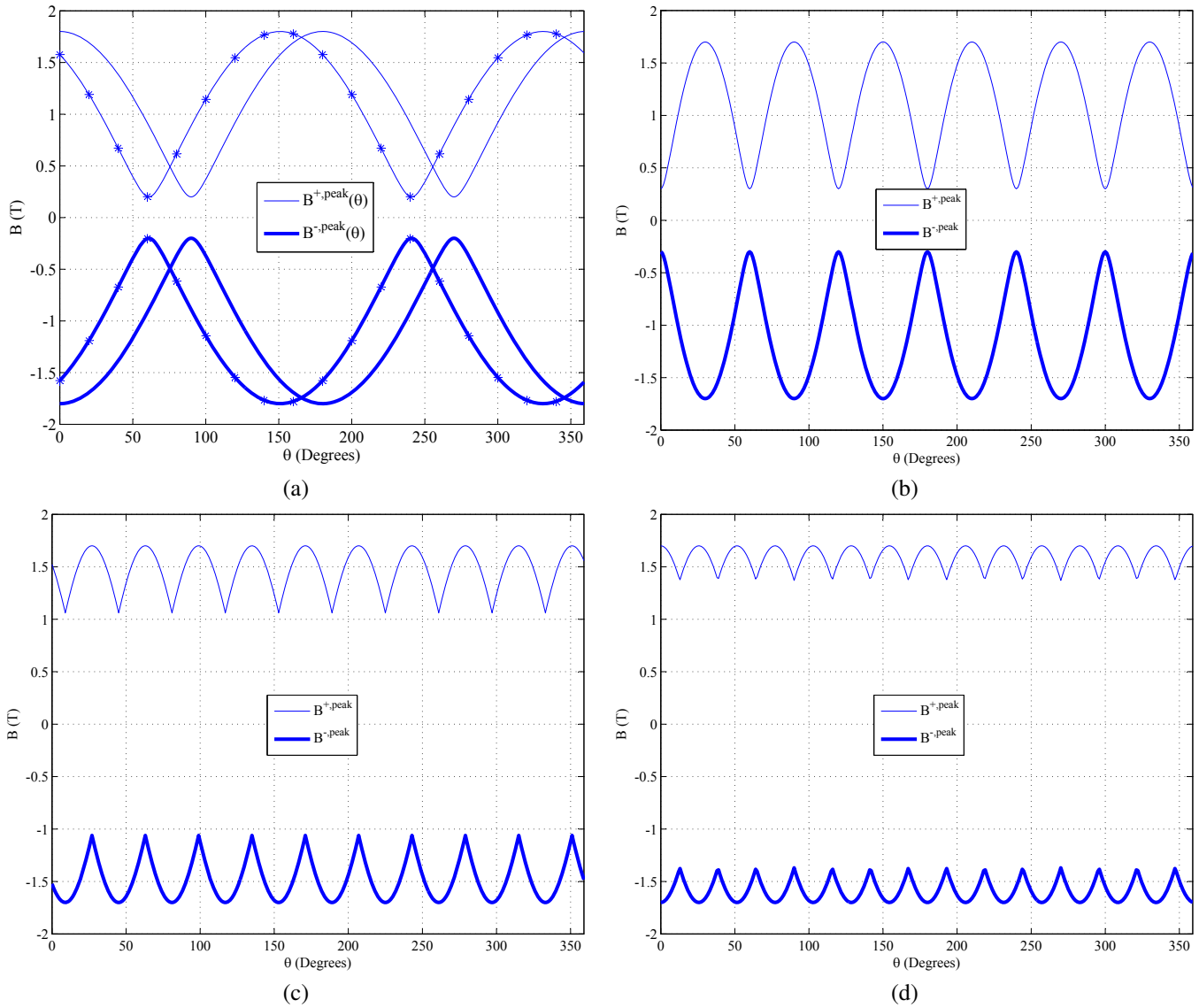

Fig. 6. Graphical representation of the negative peak values ($B^{-,\text{peak}}(\theta)$) and positive peak values ($B^{+,\text{peak}}(\theta)$) of equation (1) as a function of θ for: (a) $f_2 = f_1$, for alpha values equal to 0 and $\pi/6$ (*) radians (b) $f_2 = -f_1$, (c) $f_2 = f_1/2$ and (d) $f_2 = -f_1/2$.

opposite senses. The field distribution from a stator perspective will therefore exhibit all the characteristics presented in section III; i.e. the field distribution form changes as a function of time (Fig. 2) except at speeds corresponding to values of f_1 and f_2 that satisfy equation (4).

This latter characteristic is shown for the case satisfying section III-C by comparing the negative and positive peak flux density values computed across similar locations on different stator teeth and stator core back sections using a time-stepping finite element model of a prototype frame size D180 BDFIM operating at a speed with $f_2 = f_1/2$. The time-stepping finite element simulation was performed following the approach in [15] and the flux densities, B, in the teeth and core back section were computed using the following equation:

$$B = \frac{\Phi}{\mathrm{A}} \tag{8}$$

where A is the appropriate cross-sectional area and Φ is the magnetic flux. Peak values are shown in Fig. 7 where it can be seen that the peak flux density values vary periodically with angular position as in Fig. 6(b).

The nature of the stator field distribution is such that peak flux densities can occur at any angular position, excepting the restrictive special cases. Therefore, the stator construction has to be conventional with uniformly distributed teeth and slots. However, the analysis of saturation behaviour is notably more complex than in a conventional machine as has been found in practice [16]. The hysteresis component of the core losses cannot be predicted using Steinmetz's equation [17] as the field distribution is non-sinusoidal or has a DC-offset so the value must be computed directly from the area of the hysteresis loop, which may be predicted using a hysteresis model [18]. The assumption that is commonly made when developing thermal models of electrical machines that all teeth and core back sections rise to equal temperatures [19] is not necessarily valid when modelling operating conditions where the excitation frequencies satisfy the conditions of sections

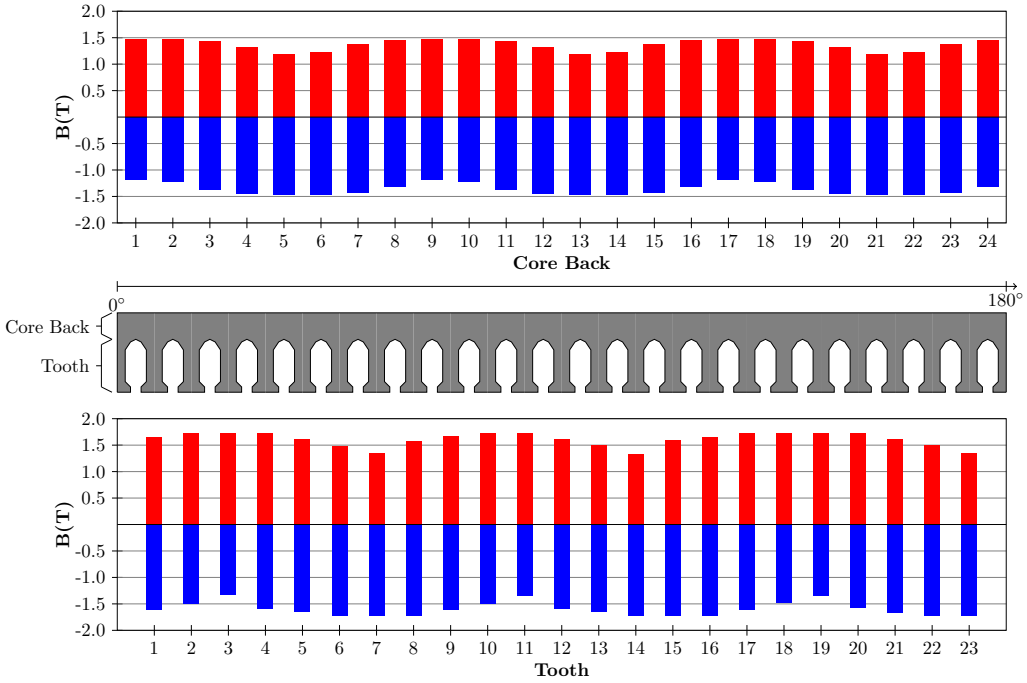

Fig. 7. The computed negative and positive peak flux density values of different stator teeth and core back sections aligned to corresponding teeth and core back sections for a finite element mode of frame size D180 BDFIM operating at 750 rev./min. with $f_1 = 50$ Hz and $f_2 = 25$ Hz at no load.

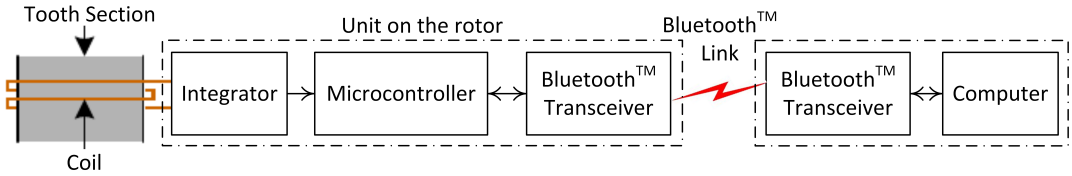

Fig. 8. System for measuring rotor flux density on the 250 kW BDFIM.

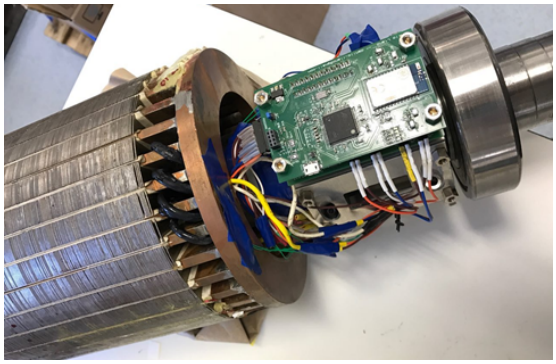

Fig. 9. System for measuring rotor flux density on the 250 kW BDFIM.

III-A and III-C as core loss will vary across different teeth and core back sections. Special consideration must go into the process of determining peak values from field distribution results obtained by simulation and by measurement as these peak values are position and load angle dependent.

B. Rotor Field Distribution Characteristics and Implications

The rotor current corresponding to the $2p_1$-pole and $2p_2$-pole field components is single frequency when the BDFIM operates in the synchronous or cascade modes [20]. Also, the relative space phase difference between the $2p_1$-pole and $2p_2$-pole field components is fixed because they are generated by the same winding. As noted on early work, the tooth flux densities depend on angular position as shown in Fig. 6(a) and Fig. 6(b); these are of course time varying at rotor current frequency. Maximum values occur at fixed angular locations. The above characteristics have been confirmed experimentally by comparing the positive and negative peak flux density values in the rotor teeth and core back sections of two BDFIMs computed using finite element analysis with measured values. Both the frame size D180 and the 250 kW BDFIMs considered have 4-pole and 8-pole stator windings and a nested loop type of rotor whose details are given in Table I, using the approach in [16]. The flux density values were measured using a single turn flux coil wound around the tooth and core back sections. The voltage signal from the coil is integrated, sampled using a microcontroller and transmitted to a computer for processing using a Bluetooth™ link, which means that flux density values

TABLE I
DETAILS OF A NESTED LOOP ROTOR FRAME SIZE OF D180 BDFM AND 250 KW BDFIM.

Parameter	**Value**	
	D180 BDFM	250 kW BDFIM
Frame size	D180	D400
No. Rotor Slots	36	60
No. Stator Slots	48	72
No. Loops per. Nested Loop Set	3	5

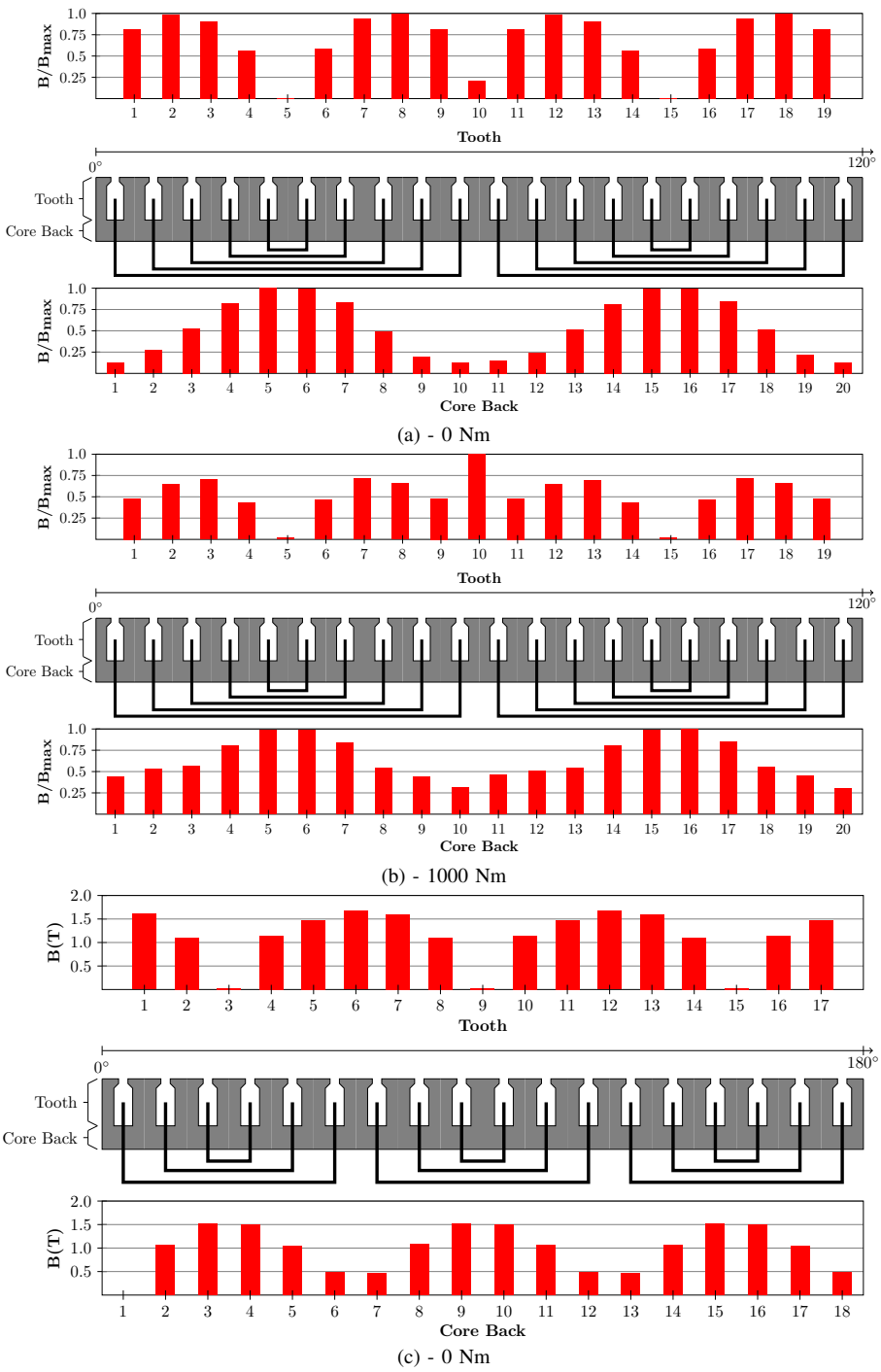

Fig. 10. The computed negative and positive peak flux density values of different teeth and core back sections shown aligned to corresponding teeth and core back sections, for: (a) and (b) - the 250 kW BDFIM operating at 625 rev./min. with $f_1 = 50$ Hz and $f_2 = 12.5$ Hz under different load conditions, and (c) the frame size D180 BDFIM operating at 750 rev./min. with $f_1 = 50$ Hz and $f_2 = 25$ Hz at no load.

can be measured even when the rotor is rotating. A diagram of the rotor flux density measurement system is shown in Fig. 8, while the system installation and signal conditioning board was presented in Fig. 9 [21]. The computed and measured flux density values are shown in Fig. 10 and Fig. 11(b), respectively. The computed flux density peak values of the different teeth and core back sections are not all equal and their variation with angular position is consistent with that in Fig. 6(b). However, the computed flux density peak values in the teeth of the 250 kW BDFIM showed a variation of flux density peak values as a function of rotor tooth and core back section number, and thus angular position, which does not fully follow the expected sinusoidal profile, attributed to the redistribution of flux caused by heavy saturation of the teeth. Additionally, the locations where the maximum and minimum peak rotor flux density peak values occur are the same for the 250 kW BDFIM and the frame size D180 BDFIM. The minimum core back and rotor tooth flux density peak values

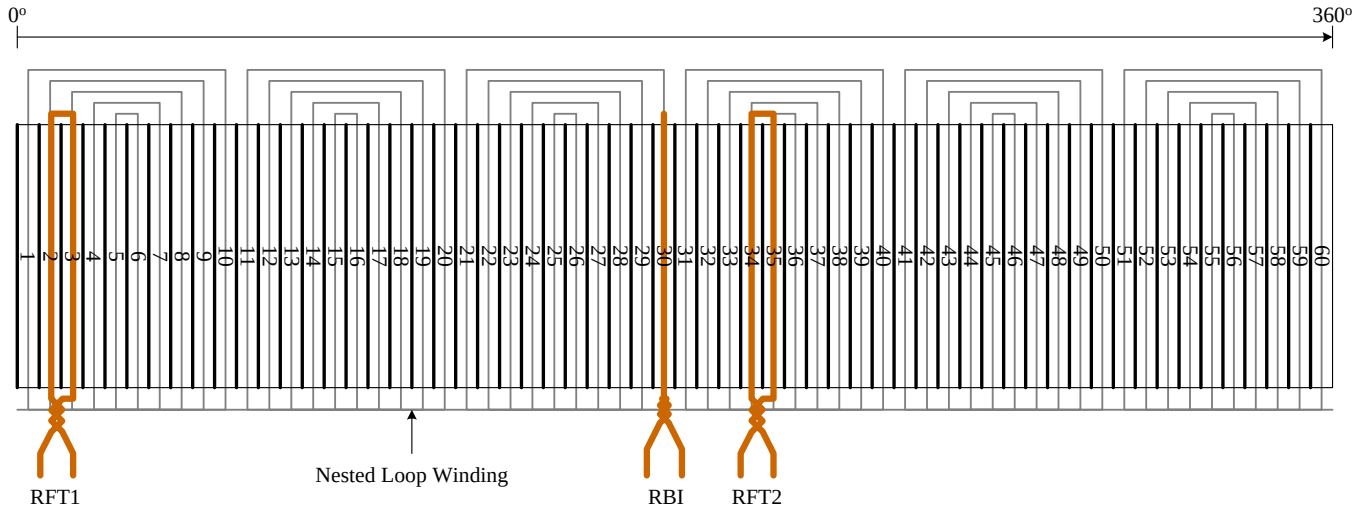

(a)

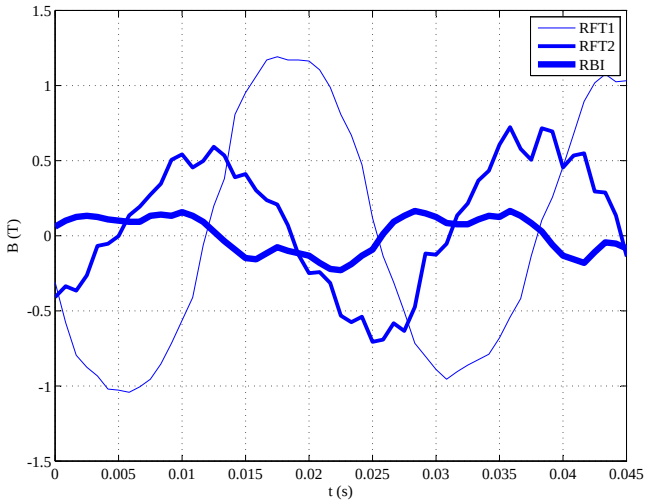

(b)

Fig. 11. (a) - The location of search coils fitted on the 250 kW nested loop rotor BDFIM. RBI is the coil around the core back section of slot number 30, RTH1 and RTH2 are the flux coils around the rotor tooth numbers 3 and 35, respectively. The thick black lines represent the teeth. (b) - The measured flux density waveforms of two teeth and a core back section of the 250 kW BDFIM rotor at the locations shown in (a) with the excitation voltage of each stator winding set equal to 690 V and the machine operating at 680 rev./min. with a load torque of 3679 Nm.

are those measured across core back sections (Fig. 11(a)) between slots with conductor sections of the outer most loops of adjacent nested loop sets and teeth with the inner loop of each nested loop set.

Different operating conditions were used for the 250 kW BDFIM regarding the measured and computed flux density values. It is easy to appreciate that flux coil RBI in Fig. 11(b) measures the minimum flux density even though there is no other flux density measurement to compare with because the location on the core where the flux density was measured is consistent with the predicted location on the core back where the flux density is a minimum, and the peak flux density value measured with flux coil RFT1 was always greater than that measured with flux coil RFT2; also in agreement with predictions.

The implications of the above characteristics are that the BDFIM rotor core need not have teeth and core back sections of equal width. However, future research needs to address the rotor redesign and optimization of rotor iron in order to reduce the machine mass by removing the redundant iron. In the case of the core loss values of different teeth and core back sections of a BDFIM with teeth and core back sections of equal width are not equal because the core loss values depend on the magnitude of the flux density. This must be taken into consideration when determining the temperature rise of rotor components either by experiment or through modelling.

V. Conclusions

An analysis of the BDFIM has been carried out to determine the characteristics of the air-gap field distribution. The analysis was based on summing the two field components and the validity of the approach has been confirmed by experimental measurements in the machine and together with their impact the design of the machine. It has been found that:

1) The rotor and stator respective reference frames field distribution characteristics are generally different and that the stator field distribution characteristics depend on the combination of stator winding excitation frequencies and thus rotor speed as per equation (7).
2) The field distribution in the stator reference frame is always a non-sinusoidal function of angular position for different time instants, and it is also a non-sinusoidal function of time for different angular positions except when the stator winding excitation frequencies are equal or when either stator winding excitation frequency is equal to zero.
3) The field distribution form changes as a function of time always on the rotor and for most combinations of stator winding excitation frequencies except the combination that results in the two field distributions having the same angular velocity.
4) The peak flux density values experienced in the teeth and core back sections of the rotor, and those of the stator at specific rotor speeds, are not all equal.

ACKNOWLEDGEMENTS

The authors would like to thank the Bradlow Foundation and St John's College at the University of Cambridge for financial assistance.

REFERENCES

[1] R. McMahon, X. Wang, E. Abdi, P. Tavner, P. Roberts and M. Jagiela, "The brushless DFIG as a generator in wind turbines," *Power Electronics and Motion Control Conference*, pp. 1859–1865, 2006.

[2] R. McMahon, P. Roberts, X. Wang and P. Tavner, "Performance of BDFM as generator and motor," *IEE Proceedings Electric Power Applications*, vol. 153, pp. 289–299, March. 2006.

[3] J. Carroll, A. McDonald and D. McMillan, "Reliability comparison of wind turbines with DFIG and PMG drive trains," *IEEE Transactions on Energy Conversion*, vol. 30, pp. 663–670, March. 2015.

[4] H. Peng, M. Cheng, S. Ademi and M. Jovanovic, "Brushless doubly-fed machines: Opportunities and challenges," *IEEE Chinese Journal of Electrical Engineering*, vol. 4, pp. 1–17, July. 2018.

[5] A. Oraee, E. Abdi, S. Abdi, R. McMahon and P. Tavner, "Effects of rotor winding structure on the BDFM equivalent circuit parameters," *IEEE Transactions on Energy Conversion*, vol. 30, pp. 1660–1669, December. 2015.

[6] M. Hsieh, I. Lin and D. Dorrell, "An analytical method combining equivalent circuit and magnetic circuit for BDFRG," *IEEE Transactions on Magnetics*, vol. 50, November. 2014.

[7] S. Ademi, M. Jovanovic and M. Hasan, "Control of brushless doubly-fed reluctance generators for wind energy conversion systems," *IEEE Transactions on Energy Conversion*, vol. 30, pp. 596–604, 2015.

[8] T. Strous, X. Wang, H. Polinder and J. Ferreira, "Brushless doubly fed induction machines: Magnetic field analysis," *IEEE Transactions on Magnetics*, vol. 52, November. 2016.

[9] H. Gorginpour, H. Oraee and R. McMahon, "A novel modeling approach for design studies of brushless doubly fed induction generator based on magnetic equivalent circuit," *IEEE Transactions on Energy Conversion*, vol. 28, pp. 902–912, 2013.

[10] X. Wang, P. Roberts and R. McMahon, "Optimisation of BDFM stator design using an equivalent circuit model and a search method," *IET Int. Conf. on Power Elect., Machines and Drives*, pp. 606–610, 2006.

[11] S. Williamson, A. Ferreira and A. Wallace, "Generalised theory of the brushless doubly-fed machine. Part 1: Analysis," *IEE Proceedings - Electric Power Applications*, vol. 144, pp. 111–122, 1997.

[12] F. Creedy, "Some developments in multi-speed cascade induction motors," *Journal of the Institute of Electrical Engineers*, pp. 511–537, 1920.

[13] A. Arnold, "The two-speed cascade induction motor," *Journal of the Institution of Electrical Engineers*, vol. 63, pp. 1115–1122, 1925.

[14] S. Abdi, E. Abdi and R. McMahon, "Optimization of the magnetic circuit for brushless doubly fed machines," *IEEE Transactions on Energy Conversion*, vol. 30, pp. 1611–1620, 2015.

[15] M. Mathekga, S. Shiyi, T. Logan and R. McMahon, "Implementation of a PI phase angle controller for finite element analysis of the BDFM," *Proc. of the Power Electronics, Machines and Drives*, 2012.

[16] S. Abdi, D. Llano, E. Abdi and R. McMahon, "Experimental analysis of noise and vibration for large brushless doubly fed machines," *The Journal of Engineering*, 2017.

[17] C. Steinmetz, "Operating alternating motors," *US587340*, 1893.

[18] J. Pedro, A. Bastos and N. Sadowski, "Electromagnetic modelling by finite element methods," *Marcel Dekker Inc., New York*, 2003.

[19] A. Bousbaine, "An investigation into the thermal modelling of induction motors," *Department of Electronic and Electrical Engineering, University of Sheffield*, 1993.

[20] A. Wallace, R. Spee and G. Alexander, "The brushless doubly-fed machine: Its advantages, applications and design methods," *IEEE. 6th Int. Conf. Electrical Machines and Drives*, pp. 511–517, 1993.

[21] D. Llano, S. Abdi, M. Tatlow, E. Abdi and R. McMahon, "Energy harvesting and wireless data transmission system for rotor instrumentation in electrical machines," *IET Power Electronics*, vol. 10, pp. 1259–1267, 2017.